

Vector polarizability of atomic states induced by linearly polarized vortex beam: External control of magic and tune-out wavelengths

Anal Bhowmik,^{1,2,*} Narendra Nath Dutta,³ and Sonjoy Majumder^{4,†}

¹*Haifa Research Center for Theoretical Physics and Astrophysics, University of Haifa, Haifa 3498838, Israel*

²*Department of Mathematics, University of Haifa, Haifa 3498838, Israel*

³*Department of Chemical Sciences, Indian Institute of Science Education and Research Mohali, Punjab-140306, India.*

⁴*Department of Physics, Indian Institute of Technology Kharagpur, Kharagpur-721302, India.*

(Dated: September 10, 2019)

In this paper, we develop a theory for frequency dependent polarizability of an atomic state in an interaction with a focused linearly polarized vortex beam. This theory naturally produces a vector component of the valence polarizability to an atomic state, unlike interaction with paraxial linearly polarized vortex or non-vortex beam, obeying the total angular momentum conservation of the beam. The theory is employed on Sr^+ ion to precisely calculate the magic wavelengths of the clock transitions $5s_{\frac{1}{2}} \rightarrow 4d_{\frac{3}{2},\frac{5}{2}}$ and tune-out wavelengths using correlation-exhaustive relativistic coupled cluster (RCC) method. The variation of the vector polarizability with the orbital angular momentum (OAM) of the beam shows significant contributions near the resonance frequencies, and sometimes comparable to the contributions of scalar and tensor polarizabilities to determine the magic wavelengths. The external control of the magic and tune-out wavelengths with the focusing angle and OAM of the beam improves the flexibility for the advancement of trapping reliant quantum technologies.

I. INTRODUCTION

In the recent years, laser trapping and cooling of neutral atoms have been attracted significant attention to the experimentalists and achieved as an established technique in high precision spectroscopic measurements [1–3]. Along with neutral atoms, charged ions are also becoming newer species of potential interests in optical dipole trapping experiments [4–7]. However, mechanism of trapping by optical means inevitably produces respective Stark shifts in the associated energy levels of the atoms and influences the fidelity of the precision measurements. Magic wavelengths are the unique wavelengths of the external laser beam for which the differential ac Stark shift of an atomic transition vanishes effectively. Therefore, the impediment in precise spectroscopic measurements can be diminished if the atoms are confined at predetermined magic wavelengths of the laser beam. These wavelengths have significant applications in atom optics, such as atomic interferometers [8], atomic clocks [9–11] and atomic magnetometers [12].

Nevertheless, determinations of precise values of magic wavelengths of an atomic transition depend mainly on how accurately the frequency-dependent or dynamic valence polarizability (POL) values, which are basically the combination of scalar (α_V^0), vector (α_V^1) and tensor (α_V^2) POL values [1–4] of the atomic Zeeman sub-level, are calculated. In general, POL is defined in term of an off-resonant electric dipole interaction between the atom and the trapping light. The vector POL, which yields the energy shift of Zeeman sublevel, arises from the circularly

polarized external field [4, 7]. Usually, it is one of the non-magnetic field sources to remove Zeeman degeneracy and becomes very significant in the evaluation of magic wavelengths for cases such as "knob" to adjust an optical trap [18]. Especially, our recent work [7] about the interaction with circularly polarized non-paraxial vortex beam shows that the magic wavelengths of an atomic transition are significantly affected by the focusing angle both in numbers and values compared to the Gaussian beam. The distinctive feature of the vortex beam is that in addition to the spin angular momentum (SAM) associated with the polarization, it has OAM which arises due to the helical phase front of the beam [19–23]. Therefore, for a circularly polarized vortex beam, it is obvious that the beam creates a vector part of the POL when it interacts with the cold atoms or ions which are below their recoil limit. However, this is not usually true for a linear polarized gaussian or vortex beam.

In this work, we show that vector POL can be produced naturally in cold atoms or ions due to interaction with a linearly polarized focused vortex (LP-FV) beam satisfying the conservation of total angular momentum of the beam. Therefore, this is one of the prolific artifacts of spin-orbit coupling in vortex beam. We apply this theory for the precise calculations of dynamic POL and as a consequence the magic wavelengths of $5s_{\frac{1}{2}} \rightarrow 4d_{\frac{3}{2},\frac{5}{2}}$ transitions of Sr^+ ion, an well studied [24–27] excellent candidates for optical frequency standard and quantum information storage [28, 29]. As the spin-orbit coupling of light depends on the topological charge and focusing angle, we quantify the effects of these parameters on the vector POL, dipole POL, magic and tune-out (where the dynamic POL goes to zero for certain frequency [30, 31]) wavelengths which will be important for experimentalists to choose the parameters of the vortex beams used

* abhowmik@campus.haifa.ac.il

† sonjoym@phy.iitkgp.ernet.in

for trapping.

II. THEORY

According to the time-independent second-order perturbation theory [5], the ac Stark shift of an atomic state in an external oscillating electric field $\mathcal{E}(\omega)$ is expressed by $\Delta F(\omega) = -\frac{1}{2}\alpha^T(\omega)\mathcal{E}^2$, where $\alpha^T(\omega)$ is the total dynamic POL of the atomic energy state at frequency ω and \mathcal{E} is the magnitude of the external electric field. In case of a single-valence atomic system with a valence electron in the ν th orbital, the total POL can be written as $\alpha^T(\omega) = \alpha^C(\omega) + \alpha^{VC}(\omega) + \alpha^V(\omega)$. Here $\alpha^C(\omega)$ is the frequency dependent core POL of the ionic core in the absence of the valence electron. $\alpha^{VC}(\omega)$ gives a correction [6] to the core POL due to the presence of the valence electron and it is considered as ω -independent in the present work due to tightly bound core electrons. $\alpha^V(\omega)$ is the valence POL of the monovalent system. The α^C and α^{VC} , relatively weaker contributing terms to total polarizability compare to α^V , are approximately computed using lower-order many-body perturbation theory discussed in references [5, 34]

Our primary focus in this paper is to evaluate $\alpha^V(\omega)$ precisely for a monovalent atomic system in the presence of an external LP-FV beam. As Laguerre-Gaussian (LG) beam is a well established example of vortex beams, we assume initially paraxial form of a linearly polarized coherent LG beam without any off-axis node and it is propagating along the z -axis. The field is expressed as [20] $\mathcal{E}_i(\rho, \phi, z, t) = \mathcal{E}_i(t) (\sqrt{2}\rho/w_0)^{|l|} e^{i(l\phi+k_0z)} \hat{\mathbf{x}}$. Here k_0 is the wave number, w_0 is the waist and l is the topological charge or OAM of the beam. We consider that this paraxial LG beam is focused by passing through an objective (lens) with a high numerical aperture (NA) [21]. Then the focussed LG beam interacts with a cold atom or ion whose de Broglie wavelength is large enough to experience the intensity variation of this beam. In order to take a full advantage of the high NA of the lens, we assume that w_0 overfills the entrance aperture radius. According to Kirchhoffs approximation of diffraction theory [35, 36], the consequent components of spin-orbit coupled non-paraxial linearly polarized LG beam can be expressed as

$$\mathcal{E}(\rho, \phi, z, t) = \begin{bmatrix} \mathcal{E}_x \\ \mathcal{E}_y \\ \mathcal{E}_z \end{bmatrix} = (-i)^{l+1} \mathcal{E}_0 e^{i(l\phi-\omega t)} \times \begin{bmatrix} u_l(\rho, z) + u_{l+2}(\rho, z)e^{2i\phi} + u_{l-2}(\rho, z)e^{-2i\phi} \\ -i(u_{l+2}(\rho, z)e^{2i\phi} - u_{l-2}(\rho, z)e^{-2i\phi}) \\ -i(u_{l+1}(\rho, z)e^{i\phi} - u_{l-1}(\rho, z)e^{-i\phi}) \end{bmatrix} \quad (2.1)$$

Here \mathcal{E}_x , \mathcal{E}_y and \mathcal{E}_z are the x -, y - and z - components of the electric field, respectively. The amplitude of the focused electric field is $\mathcal{E}_0 = \frac{\pi f}{\lambda} T \mathcal{E}_i$, where \mathcal{E}_i is the amplitude of the incident electric field, T is the transmission amplitude of the objective, and f is its focal length related with ρ by $\rho = f \sin \theta$ (Abbe sine

condition). The coefficients u_{l+m} , where m takes the values 0, ± 1 , ± 2 in the above expression, depends on the focusing angle of NA (ϑ_m) by [37] $u_{l+m}(\rho, z) = \int_0^{\vartheta_m} d\vartheta \left(\frac{\sqrt{2}\rho}{w_0} \right)^{|l|} \sin \vartheta \sqrt{\cos \vartheta} g_{|m|}(\vartheta) J_{l+m}(k\rho \sin \vartheta) e^{ikz \cos \vartheta}$.

Here $J_{l+m}(k\rho \sin \vartheta)$ is cylindrical Bessel function and $k = \mu k_0$, where μ is the refractive index of the medium. The angular functions, $g_{|m|}(\vartheta)$, are $g_0(\vartheta) = 1 + \cos \vartheta$, $g_1(\vartheta) = \sin \vartheta$, $g_2(\vartheta) = 1 - \cos \vartheta$.

Now, let us discuss about Eq. (2.1) in detail. Linearly polarized light can be considered as the superposition of left ($\beta = +1$) and right ($\beta = -1$) circularly polarized light. Because of focusing and the diffraction from the edges of the aperture, each circularly polarized light ($\beta = \pm 1$) can be decomposed into three sets of local polarizations (± 1 , ∓ 1 and polarization along z -axis) [21]. Among these three sets of local polarizations, the first set has equal amplitude (u_l) for ± 1 local polarizations. Therefore, even after passing through the focusing lens, the superposition of these local polarizations results linearly polarized beam with the OAM similar to the OAM of the incident beam. However, in the case of second set, different field amplitudes, u_{l+2} and u_{l-2} , are generated with two different polarizations and topological charges ($l+2$ and $l-2$, respectively,) after focusing and conserving the total angular momentum of the beam. Therefore, the field will gain from two opposite circular polarizations having different amplitudes and creates the vector part of valence POL in interaction with an atomic systems. Further, the third set yields u_{l+1} and u_{l-1} fields with topological charges $l+1$ and $l-1$, respectively; but both the fields are polarized along the z -direction, which is another interesting manifestations of focusing the beam. Nevertheless, using the non-paraxial form of linearly polarized electric field presented in Eq. (2.1), $\alpha^V(\omega)$ of an atomic system can be expressed as $\alpha^V(\omega) = C_0 \alpha_V^0(\omega) + C_1 \alpha_V^1(\omega) + C_2 \alpha_V^2(\omega)$. Here the coefficients C_i s are expressed in the following forms: $C_0 = \{u_l\}^2 + \{u_{l+1}\}^2 + \{u_{l-1}\}^2 + 2[\{u_{l+2}\}^2 + \{u_{l-2}\}^2]$, $C_1 = [2\{u_{l-2}\}^2 - 2\{u_{l+2}\}^2] \times \left(\frac{m_{J_V}}{2J_V} \right)$, and $C_2 = [\{u_l\}^2 - \{u_{l+1}\}^2 - \{u_{l-1}\}^2 + 2\{u_{l+2}\}^2 + 2\{u_{l-2}\}^2] \times ((3m_{J_V}^2 - J_V(J_V + 1))/(2J_V(2J_V - 1)))$, where J_V and m_{J_V} are the total angular momentum and its magnetic component for the single-valence atomic state $|\Phi_V\rangle$. The calculation of $\alpha^V(\omega)$ [5, 7] of an atomic state directly depends on different combinations of integrals u_{l+m} . These integrals can be altered with the various choices of the topological charges of the incident LG beam and the NA of the objective. As a consequence, the total POL of an atomic state and associated magic wavelengths of transitions can be tuned externally using different structures of the beam.

III. NUMERICAL RESULTS AND DISCUSSIONS

As the electron-correlation affects the α^V part of dynamic POL most significantly due to a loosely bound valence electron, the precise estimations of the scalar, vector and tensor parts of the valence POL for the corresponding states require correlation exhaustive many-body calculations [8–15] with a sophisticated numerical approach. The reader is requested to see the ‘Supplementary Material’ (SM) of this paper. Whereas, the core polarizability, $\alpha^C(\omega)$, is valence-state independent quantity and can be calculated quite accurately with core polarization corrected $E1$ matrix elements using the 2nd-order relativistic many-body perturbation theory [46]. Our calculation yields that the static core POL ($\alpha^C(0)$) of the ion is 6.103 a.u.. The static core-valence parts of the POL ($\alpha^{VC}(0)$) for the states $5s_{\frac{1}{2}}$, $4d_{\frac{3}{2}}$ and $4d_{\frac{5}{2}}$ are -0.25 a.u., -0.38 a.u. and -0.42 a.u., respectively [7]. By employing the many-body methods as indicated above, the static scalar POL ($\alpha_V^0(0)$) of $5s_{\frac{1}{2}}$, $4d_{\frac{3}{2}}$ and $4d_{\frac{5}{2}}$ states are found to be 87.68 a.u., 55.92 a.u. and 56.21 a.u., respectively [7], and static tensor POL ($\alpha_V^2(0)$) of $4d_{\frac{3}{2}}$ and $4d_{\frac{5}{2}}$ states become -34.67 a.u. and -47.12 a.u., respectively [7].

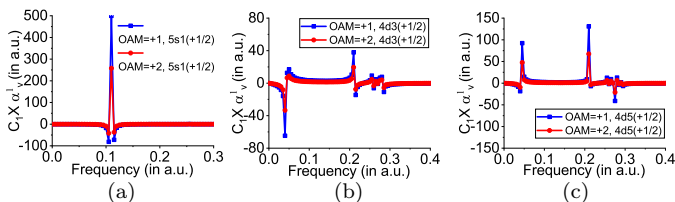


FIG. 1. Frequency dependence of total vector POL ($C_1\alpha_V^1$) of the $5s_{\frac{1}{2}}(+1/2)$ and $4d_{\frac{3}{2},\frac{5}{2}}(+1/2)$ states for the LG beam having linear polarization are displayed at focusing angle 60° .

In Fig 1, graphical variations of total vector POL ($C_1\alpha_V^1(\omega)$) of $5s_{\frac{1}{2}}(+1/2)$ and $4d_{\frac{3}{2},\frac{5}{2}}(+1/2)$ states of Sr^+ are plotted with the frequency to have quantitative analysis ($m_J = -\frac{1}{2}$ will give opposite sign of vector POL). Here the incident LG beam is considered with OAM=+1 and +2 with the focusing angle of 60° ; though the variation of $C_1\alpha_V^1(\omega)$ with the focusing angle is marginal here. However, the focusing angle has significant effects on the scalar and tensor POL, and consequently on the total POL (discussed later). As shown in this figure, all the magnetic sublevels of $5s_{\frac{1}{2}}$ and $4d_{\frac{3}{2},\frac{5}{2}}$ states have positive as well as negative vector POL values in the presented frequency spectrum. The peak values of the vector POL occur at resonance frequencies: 0.11 a.u. for $5s_{\frac{1}{2}}$; around 0.045 a.u and 0.21 a.u. for $4d_{\frac{3}{2},\frac{5}{2}}$ states. As expected and also it is clear from the graphs that OAM=+1 always produces higher peak value of vector POL compare to OAM=+2 as dipole matrix elements induced by the former is much stronger than the later. Also, the magnitude of the peak value of the vector POL is magnified with m_J for a fixed value of J , which is obvious from the

expression of C_1 (also see SM). Many small scale structures in the vector POL profile of $4d_{\frac{3}{2},\frac{5}{2}}$ arises due to multiple number of resonance transitions.

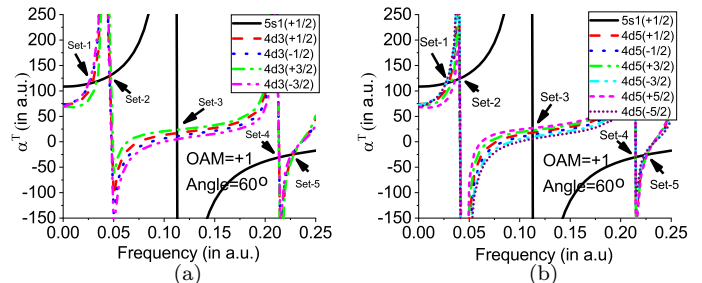


FIG. 2. Frequency dependence of α^T for the $5s_{\frac{1}{2}}$ and $4d_{\frac{3}{2},\frac{5}{2}}$ states for the linearly polarized focused (60°) LG beam with OAM=+1 are presented. The parentheses indicate the magnetic components. The wavelengths at the intersections of the polarizability curves of the $5s_{\frac{1}{2}}$ and $4d_{\frac{3}{2},\frac{5}{2}}$ states are magic wavelengths. For all the clock transitions, five sets of magic wavelengths are found.

The plots in Fig. 2 display the total dynamical POL profiles of $5s_{\frac{1}{2}}$ and $4d_{\frac{3}{2},\frac{5}{2}}$ states at 60° focusing angle of the LG beam with OAM=+1. Here, due to focusing, the light induces spin-orbit couplings which affects the total scalar ($C_0\alpha_V^0$), vector ($C_1\alpha_V^1$) and tensor ($C_2\alpha_V^2$) POL values. These plots show a number of intersection points between the POL profiles of the multiplets of $5s_{\frac{1}{2}}$ and $4d_{\frac{3}{2},\frac{5}{2}}$ states. These intersection points are the magic wavelengths at which the differential ac-Stark shift of the associated clock transition states vanishes. The figure shows that there are five sets (Set-1 to Set-5) of magic wavelengths for $5s_{\frac{1}{2}} \rightarrow 4d_{\frac{3}{2},\frac{5}{2}}$ transitions at each set of the magnetic sublevels. The magic wavelengths are spanned from the near-infrared to the UV regions of the electromagnetic spectrum (details are given in the SM along with the direct evidence of spin-orbit coupling). One can see from the plots that the magic wavelengths which falls at the infrared regions correspond to larger values of total POL. Therefore, these magic wavelengths are the most important to trap the ion and support the red-detuned trapping scheme.

The dependency of OAM and focusing angle of the beam on the properties of atoms, such as magic wavelengths along with corresponding total and vector POL values for the $5s_{\frac{1}{2}} \rightarrow 4d_{\frac{5}{2}}(+3/2)$ transition, are presented in FIG. 3 and FIG. 4 for the cases Set-1, Set-2 and Set-3 as indicated in FIG. 2(b). The magic wavelengths and total POL values of the Set-1, Set-2 and Set-3 are (1793.83 nm, 99.14 a.u.), (1119.49 nm, 107.13 a.u.) and (407.18 nm, 14.02 a.u.), respectively, for linearly polarized paraxial LG beam. The presented results for paraxial cases are also true for Gaussian beam as the OAM of the LG beam does not affect the electronic motion of an cold atom or ion (which is below its recoil limit) at the dipole transition level [20] and accordingly OAM does not influence the dipole POL of an atomic state under the paraxial limit [7]. Effective contributions of vector POL to the total POL values, presented in Fig. 4(a) and (b), show

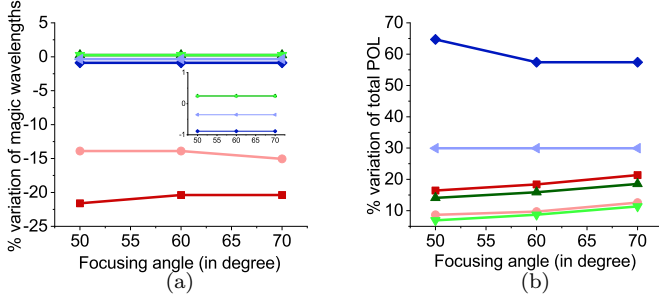


FIG. 3. Percentage variations of (a) magic wavelengths and (b) corresponding total POL values are presented with respect to focusing angles for the $5s_{\frac{1}{2}} \rightarrow 4d_{\frac{3}{2}}(+3/2)$ transition. Set-1, Set-2 and Set-3 data of FIG. 2(b) are considered here. The variation is determined by comparing the data with linearly polarized paraxial LG beam. Here red, light red, green, light green, blue and light blue colors are for (Set-1, OAM=+1), (Set-1, OAM=+2), (Set-2, OAM=+1), (Set-2, OAM=+2), (Set-3, OAM=+1), and (Set-3, OAM=+2), respectively. Inset of figure (a) shows the same plots for latter three colors but in the different range of vertical axis.

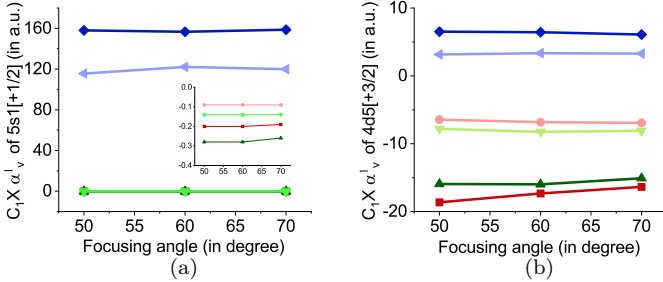


FIG. 4. Variation of three sets (at magic wavelengths of Set-1, Set-2 and Set-3 of fig. 3(a)) of vector POL (in a.u.) of (a) $5s_{\frac{1}{2}}(+1/2)$ and (b) $4d_{\frac{3}{2}}(+3/2)$ for OAM=+1 and +2 with focusing angle (degree) are presented. Colors are as mentioned in fig. 3. Inset of fig. (a) shows the same plot but in different range of and vertical axis.

that vector POL values are extremely important only at magic wavelengths near 407 nm for $5s_{\frac{1}{2}}$ state. Whereas, the vector POL is significant at all the magic wavelengths for $4d_{\frac{3}{2}}$, specially at IR wavelengths. Further point to notice that vector POL have marginal dependence on the focusing angle. It is clear from Fig. 3(b) and Fig. 4 that for a particular set, the increase of OAM decreases the total POL and corresponding magnitude of vector POL and these are true for all wavelengths.

FIG. 5 illustrates the wavelength dependence dynamic POL values of the state $4d_{\frac{3}{2}}$ of Sr^+ due to the external field of LG beam with OAM=+1 and +2, focused at angle 60° as well as for the paraxial Gaussian beam. Here, both the beams are linearly polarized. As the Gaussian beam is paraxial, there will not be any vector part in the total POL and the tune out wavelengths for $4d_{\frac{3}{2}}(|1/2\rangle)$ and $4d_{\frac{3}{2}}(|3/2\rangle)$ are 507.83 nm and 744.12 nm, respectively. It is already found in the literature that inclusion

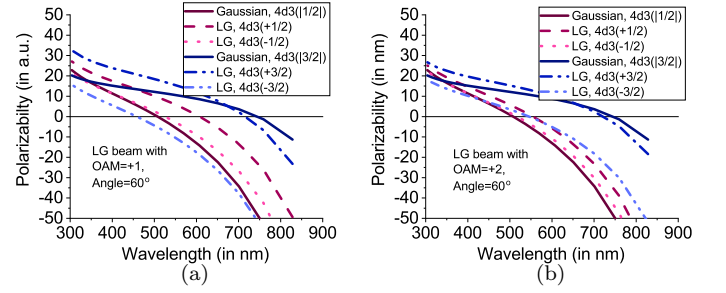


FIG. 5. Variation of total POL (in a.u.) with wavelength (in nm) for the all the magnetic components of the state $4d_{\frac{3}{2}}$ for LG beam focused at 60° (with (a) OAM=+1 and (b) +2) and paraxial Gaussian beam are presented. Wavelengths at which the curves intersects zero-polarizability axis are called tune out wavelengths.

of vector POL for circularly polarized paraxial Gaussian beam, creates an equal amount of shift to the tune out wavelengths in opposite direction [47]. But, here the vector POL is generated due to the focusing of linearly polarized LG beam and it shifts the tune out wavelength differently for different multiplets. For $4d_{3/2}$ state, both $m_J = \pm 1/2$ sublevels shifts towards larger wavelengths for OAM=+1 and +2. Whereas, for $m_J = \pm 3/2$ sublevels, tune out wavelengths shift towards smaller wavelengths. Moreover, the separation of tune out wavelengths corresponding to the sublevels of particular multiplets decreases with the increase of OAM of the beam, which indicates the effect of the spin-orbit coupling varies with topological charge of the vortex beam. All the magic and tune out wavelengths calculated in this paper have maximum uncertainty of around $\pm 1\%$. Details of this uncertainty estimation procedure is discussed in Ref.[7].

IV. CONCLUSION

In summary, we have developed a theoretical formalism for the dynamical POL values of the atomic states due to linearly polarized non-paraxial vortex beam. The significant influences of vector polarizabilities to these dynamical POL values for this linearly polarized light, which is absent for gaussian beam or even for paraxial vortex beam, is one of the main findings of this work. This formalism is explored to calculate the magic wavelengths of the clock transitions $5s_{\frac{1}{2}} \rightarrow 4d_{\frac{3}{2}, \frac{5}{2}}$ of the Sr^+ ion. Moreover, the effects of topological charges and spin-orbit coupling as focusing angle of the vortex beam are studied to investigate the variation of the total POL values and eventually on the magic wavelengths. A large numbers of magic wavelengths, shown for the clock transitions of Sr^+ ion, can be useful to restrict the ion's position following a blue- or red-detuned trapping scheme. The tunability of the magic wavelengths proves that the spin-orbit coupling of the LG beam adds an extra freedom to control an atom or ion. The vector POL values

presented in this paper can be verified experimentally by stimulated Raman spectroscopy [48] or by measuring the tune-out wavelengths for magnetic sublevels of same multiplets [47, 49]. We believe that the present theo-

retical development will give an additional flexibility to trap an atom or ion using red- or blue-detuned trapping technique in near future.

-
- [1] C. Champenois, M. Houssin, C. Lisowski, M. Knoop, G. Hagel, M. Vedel, and F. Vedel, *Phys. Lett. A* **331**, 298 (2004).
- [2] C. W. Chou, D. B. Hume, J. C. J. Koelemeij, D. J. Wineland, and T. Rosenband, *Phys. Rev. Lett.* **104**, 070802 (2010).
- [3] A. D. Ludlow, M. M. Boyd, J. Ye, E. Peik, and P. O. Schmidt, *Rev. Mod. Phys.* **87**, 637 (2015).
- [4] T. Lauprêtre, R. B. Linnet, I. D. Leroux, H. Landa, A. Dantan, and M. Drewsen, *Phys. Rev. A* **99**, 031401(R) (2019).
- [5] J. Schmidt, A. Lambrecht, P. Weckesser, M. Debatin, L. Karpa, and T. Schaetz, *Phys. Rev. X* **8**, 021028 (2018).
- [6] A. Lambrecht, J. Schmidt, P. Weckesser, M. Debatin, L. Karpa, and T. Schaetz, *Nat. Photonics* **11**, 704 (2017).
- [7] T. Schaetz, *J. Phys. B: At. Mol. Opt. Phys.* **50**, 102001 (2017).
- [8] G. W. Biedermann, X. Wu, L. Deslauriers, S. Roy, C. Mahadeswaraswamy, and M. A. Kasevich, *Phys. Rev. A* **91**, 033629 (2015).
- [9] H. S. Margolis, *J. Phys. B* **42**, 154017 (2009).
- [10] T. Nicholson, S. Campbell, R. Hutson, G. Marti, B. Bloom, R. McNally, W. Zhang, M. Barrett, M. Safronova, G. Strouse *et al.*, *Nat. Commun.* **6**, 6896 (2015).
- [11] P. Rosenbusch, S. Ghezali, V. A. Dzuba, V. V. Flambaum, K. Bely, and A. Derevianko, *Phys. Rev. A* **79**, 013404 (2009).
- [12] R. C. Dong, R. Wei, Y. B. Du, F. Zou, J. D. Lin, and Y. Z. Wang, *Appl. Phys. Lett.* **106**, 152402 (2015).
- [13] B. Arora, M. S. Safronova, and C. W. Clark, *Phys. Rev. A* **76**, 052509 (2007).
- [14] C. Lacroite, K. S. Choi, A. Goban, D. J. Alton, D. Ding, N. P. Stern, H. J. Kimble, *New J. Phys.* **14**, 023056 (2012).
- [15] B. Arora and B. K. Sahoo, *Phys. Rev. A* **86**, 033416 (2012).
- [16] V. V. Flambaum, V. A. Dzuba, and A. Derevianko, *Phys. Rev. Lett.* **101**, 220801 (2008).
- [17] A. Bhowmik, N. N. Dutta, and S. Majumder, *Phys. Rev. A* **97**, 022511 (2018).
- [18] H. Kim, H. S. Han, and D. Cho, *Phys. Rev. Lett.*, **111**, 243004 (2013).
- [19] L. Allen, M. W. Beijersbergen, R. J. C. Spreeuw, and J. P. Woerdman, *Phys. Rev. A* **45**, 8185 (1992).
- [20] P. K. Mondal, B. Deb, S. Majumder, *Phys. Rev. A* **89**, 063418 (2014).
- [21] A. Bhowmik, P. K. Mondal, S. Majumder, and B. Deb, *Phys. Rev. A* **93**, 063852 (2016).
- [22] C. T. Schmiegelow, J. Schulz, H. Kaufmann, T. Ruster, U. G. Poschinger, and F. Schmidt-Kaler, *Nature Communications* **7**, 12998 (2016).
- [23] A. Bhowmik and S. Majumder, *J. Phys. Commun.* **2**, 125001 (2018).
- [24] H. S. Margolis, G. P. Barwood, G. Huang, H. A. Klein, S. N. Lea, K. Szymaniec, and P. Gill, *Science* **306**, 1355 (2004).
- [25] J. P. Likforman, V. Tugayé, S. Guibal, and L. Guidoni, *Phys. Rev. A* **93**, 052507 (2016).
- [26] H. Zhang, M. Gutierrez, G. H. Low, R. Rines, J. Stuart, T. Wu and I. Chuang, *New J. Phys.* **18** 123021 (2016).
- [27] G. P. Barwood, G. Huang, H. A. Klein, L. A. M. Johnson, S. A. King, H. S. Margolis, K. Szymaniec, and P. Gill, *Phys. Rev. A* **89**, 050501(R) (2014).
- [28] N. Akerman, N. Navon, S. Kotler, Y. Glickman, and R. Ozeri, *New J. of Phys.* **17**, 113060 (2015).
- [29] Y. Shapira, R. Shaniv, T. Manovitz, N. Akerman, and R. Ozeri, *Phys. Rev. Lett.* **121**, 180502 (2018).
- [30] L. J. LeBlanc and J. H. Thywissen, *Phys. Rev. A* **75**, 053612 (2007).
- [31] X. Wang, J. Jiang, L. -Y. Xie, D. -H. Zhang, and C. -Z. Dong, *Phys. Rev. A* **94**, 052510 (2016).
- [32] J. Mitroy, M. S. Safronova, and C. W. Clark, *J. Phys. B: At. Mol. Opt. Phys.* **43**, 202001 (2010).
- [33] N. N. Dutta, S. Roy, and P. C. Deshmukh, *Phys. Rev. A* **92**, 052510 (2015).
- [34] T. K. Ghosh, A. K. Das, M. Castro, S. Canuto, and P. K. Mukherjee, *Phys. Rev. A* **48**, 2686 (1993).
- [35] B. Richards and E. Wolf, *Proc. R. Soc. London, Ser. A* **253**, 358 (1959).
- [36] A. Boivin and E. Wolf, *Phys. Rev.* **138**, B1561 (1965).
- [37] Y. Zhao, J. S. Edgar, G. D. M. Jeffries, D. McGloin, and D. T. Chiu, *Phys. Rev. Lett.* **99**, 073901 (2007).
- [38] I. Lindgren and J. Morrison, *Atomic Many-body Theory*, ed. G. E. Lambropoulos and H. Walther (3rd ed.; Berlin: Springer), 3 (1985).
- [39] R. F. Bishop, and H. G. Kummel, *Physics Today* March **40**, 52 (1987).
- [40] I. Lindgren, and J. Morrison, *Atomic Many-Body Theory*, (Springer, 1986).
- [41] I. Lindgren, *Phys. Rev. A* **31**, 1273 (1985).
- [42] R. J. Bartlett and M. Musial, *Reviews of Modern Physics* **79**, 291 (2007).
- [43] N. N. Dutta and S. Majumder *Indian Journal of Physics* **90**, 373 (2016).
- [44] A. Bhowmik, S. Roy, N. N. Dutta, and S. Majumder, *J. Phys. B: At. Mol. Opt. Phys.* **50**, 125005 (2017).
- [45] A. Das, A. Bhowmik, N. N. Dutta, and S. Majumder, *J. Phys. B: At. Mol. Opt. Phys.* **51**, 025001 (2018).
- [46] W. R. Johnson, Z. W. Liu, and J. Sapirstein, *At. Data Nucl. Data Tables* **64**, 279 (1996).
- [47] F. Schmidt, D. Mayer, M. Hohmann, T. Lausch, F. Kindermann, and A. Wideral, *Phys. Rev. A* **93**, 022507 (2016).
- [48] Q. -Q. Hu, C. Freier, Y. Sun, B. Leykauf, V. Schkolnik, J. Yang, M. Krutzik, and A. Peters, *Phys. Rev. A* **97**, 013424 (2018).
- [49] R. Trubko, M. D. Gregoire, W. F. Holmgren, and A. D. Cronin, *Phys. Rev. A* **95**, 052507 (2017).

SUPPLEMENTARY MATERIALS (SM)

V. EXPRESSIONS OF SCALAR, VECTOR, TENSOR AND TOTAL VALENCE POLARIZABILITY:

$\alpha_V^0(\omega)$, $\alpha_V^1(\omega)$, and $\alpha_V^2(\omega)$ are the scalar, vector, tensor parts, respectively, of the dynamic valence polarizability $\alpha^V(\omega)$ which are expressed in sum-over-states approach [1–6] as follows

$$\alpha_V^0(\omega) = \frac{2}{3(2J_V + 1)} \sum_N \frac{|\langle \psi_V || d || \psi_N \rangle|^2 \times (\epsilon_N - \epsilon_V)}{(\epsilon_N - \epsilon_V)^2 - \omega^2}, \quad (5.1)$$

$$\alpha_V^1(\omega) = -\sqrt{\frac{6J_V}{(J_V + 1)(2J_V + 1)}} \sum_N (-1)^{J_N + J_V} \begin{Bmatrix} J_V & 1 & J_V \\ 1 & J_N & 1 \end{Bmatrix} \frac{|\langle \psi_V || d || \psi_N \rangle|^2 \times 2\omega}{(\epsilon_N - \epsilon_V)^2 - \omega^2}, \quad (5.2)$$

$$\alpha_V^2(\omega) = 4\sqrt{\frac{5J_V(2J_V - 1)}{6(J_V + 1)(2J_V + 1)(2J_V + 3)}} \sum_N (-1)^{J_N + J_V} \begin{Bmatrix} J_V & 1 & J_N \\ 1 & J_V & 2 \end{Bmatrix} \frac{|\langle \psi_V || d || \psi_N \rangle|^2 \times (\epsilon_N - \epsilon_V)}{(\epsilon_N - \epsilon_V)^2 - \omega^2}, \quad (5.3)$$

and

$$\alpha^V(\omega) = C_0 \alpha_V^0(\omega) + C_1 \alpha_V^1(\omega) + C_2 \alpha_V^2(\omega). \quad (5.4)$$

Here J_V is the total angular momentum of ψ_V . $|\langle \psi_V || d || \psi_N \rangle|$ is the reduced dipole matrix elements. C_i s depend on the beam parameter.

VI. NUMERICAL PROCEDURE:

The electron-correlation significantly affects α^V of the dynamic polarizability due to the loosely bound valence electron. Therefore, the precise estimations of the scalar, vector and tensor parts of the valence polarizabilities for the corresponding states require correlation-exhaustive many-body treatments with a sophisticated numerical approach. In the process of evaluations of the valence polarizabilities for $5s_{\frac{1}{2}}$, $4d_{\frac{3}{2}}$, and $4d_{\frac{5}{2}}$ states of Sr^+ , we consider the running index N to indicate all possible non-zero dipole matrix elements in the Eq. (5.1) to (5.3) with the states up to principle quantum number 25. According to the significance of each $E1$ matrix elements to the summations in these equations, many-body calculations of different orders of correlations are employed with negligible compromise in the accuracy of estimations [7]. The most dominant $E1$ matrix elements are associated with the intermediate states $5^2P_{1/2,3/2}$ to $8^2P_{1/2,3/2}$ and $4^2F_{5/2,7/2}$ to $6^2F_{5/2,7/2}$ as ψ_N and they are computed using a relativistic coupled-cluster (RCC) theory having a closed-shell and a single-valence open-shell cluster operators containing single, double and valence triple excitations in linear and non-linear forms [8–15]. Relatively less significant dipole matrix elements are involved with the states $9^2P_{1/2,3/2}$ to $12^2P_{1/2,3/2}$ and $7^2F_{5/2,7/2}$

to $12^2F_{5/2,7/2}$ and are evaluated using the 2nd-order relativistic many-body perturbation theory. The remaining matrix elements contribute a little to the sums as defined in Eq. (5.1) to (5.3) and are calculated using the Dirac-Fock method. Also, in order to achieve a better accuracy in the magic wavelengths and the corresponding total dynamic polarizabilities, we have utilized the transition energies from the experimental data [16]. By employing the above methods, the static scalar polarizabilities ($\alpha_V^0(0)$) of $5s_{\frac{1}{2}}$, $4d_{\frac{3}{2}}$ and $4d_{\frac{5}{2}}$ states are calculated as 87.68 a.u., 55.92 a.u. and 56.21 a.u., respectively, and static tensor polarizabilities ($\alpha_V^2(0)$) of $4d_{\frac{3}{2}}$ and $4d_{\frac{5}{2}}$ states are computed as -34.67 a.u. and -47.12 a.u., respectively.

VII. LIST OF MAGIC WAVELENGTHS AND CORRESPONDING TOTAL AND VECTOR POLARIZABILITIES:

A list of magic wavelengths spanned from the near-infrared to the UV regions and the corresponding total polarizabilities of the transitions $5s_{\frac{1}{2}} \rightarrow 4d_{\frac{3}{2}, \frac{5}{2}}$ are presented in Table I to Table III. Also, at each magic wavelength, values of the vector polarizability contributions of relevant states $5s_{\frac{1}{2}}$ and $4d_{\frac{3}{2}, \frac{5}{2}}$ are presented. Results are displayed for the OAM=+1, and +2 while the focusing angles of the beam are considered as 50°, 60° and 70°. As seen in the tables, all the transitions between the magnetic sublevels of $5s_{\frac{1}{2}}$ and $4d_{\frac{3}{2}, \frac{5}{2}}$ states produce five sets of magic wavelengths except few cases of $5s_{\frac{1}{2}} \rightarrow 4d_{\frac{5}{2}}$

transition for OAM=+2. Depending on the proximity of the resonances, the strength of the vector polarizability of one of the transition states dominates over that of the other state in a total polarizability value at a magic wavelength. For $5s_{\frac{1}{2}} \rightarrow 4d_{\frac{5}{2}}(+5/2)$ transition, we have found (in table III) two sets of infrared magic wavelengths are missing at the focusing angle 50° and 60° of the beam, but all five sets of magic wavelengths present at 70° when the projected beam has OAM=+2. This highlights the direct effect of spin-orbit coupling of LG beam on the magic wavelengths. All the tables show that the magic wavelengths fall in the visible and UV region of the electromagnetic spectrum support the blue-detuned trapping scheme confining the ion in the low intensity region of the LG beam [17–20].

TABLE I. Magic wavelengths (in nm) with corresponding polarizabilities (in a.u.) of Sr^+ for different focusing angles of the focused LG beam (with OAM=+1 and +2) for the transitions $5s_{\frac{1}{2}}(+1/2) \rightarrow 4d_{\frac{3}{2}}(m_J)$. The values in the first parentheses refer vector polarizabilities of the states, $5s_{\frac{1}{2}}(+1/2)$ (left) and $4d_{\frac{3}{2}}(m_J)$ (right) at the corresponding magic wavelengths.

Non-paraxial LG beam						
State	λ^{50°	α^{50°	λ^{60°	α^{60°	λ^{70°	α^{70°
$(4d_{\frac{3}{2}}(m_J))$	OAM=+1					
$(+\frac{1}{2})$	1627.26	113.53 (-0.16, -7.20)	1598.71	115.45 (-0.16, -7.81)	1571.15	117.37 (-0.16, -7.27)
	992.67	126.99 (-0.33, 12.91)	981.97	129.94 (-0.34, 13.95)	981.97	132.77 (-0.32, 13.14)
	403.57	17.32 (158.00, 3.10)	403.57	17.32 (156.69, 3.07)	403.57	17.32 (158.72, 2.91)
	213.21	-29.88 (-0.13, -0.93)	213.21	-30.79 (-0.13, -0.84)	213.21	-31.81 (-0.13, -0.24)
	200.01	-24.11 (-0.10, -1.37)	200.45	-25.01 (-0.10, -1.43)	200.45	-26.03 (-0.09, -1.24)
$(-\frac{1}{2})$	1786.80	111.60 (-0.15, 5.20)	1752.44	114.54 (-0.15, 6.21)	1752.44	116.47 (-0.14, 5.52)
	1003.60	126.99 (-0.33, -12.51)	992.67	129.94 (-0.34, -13.25)	992.67	131.86 (-0.32, -12.93)
	403.57	10.53 (158.00, -3.10)	403.57	10.53 (156.69, -3.07)	403.57	11.54 (158.72, -2.91)
	213.21	-29.88 (-0.13, 0.93)	213.21	-30.79 (-0.13, 0.84)	213.21	-31.81 (-0.13, 0.24)
	200.45	-25.01 (-0.10, 1.47)	200.90	-25.01 (-0.10, 1.43)	201.34	-26.03 (-0.09, 1.64)
$(+\frac{3}{2})$	1368.27	116.47 (-0.19, -40.15)	1389.13	118.39 (-0.20, -37.93)	1406.28	120.32 (-0.19, -34.55)
	961.25	128.92 (-0.35, 43.73)	961.25	130.84 (-0.37, 43.90)	961.25	133.79 (-0.34, 42.50)
	403.57	23.09 (158.00, 9.25)	403.57	23.09 (156.69, 9.26)	403.57	23.09 (158.72, 8.75)
	213.21	-29.88 (-0.13, -2.78)	212.71	-30.79 (-0.13, -18.52)	213.21	-31.81 (-0.13, -2.64)
	199.58	-24.11 (-0.10, -4.33)	199.58	-25.01 (-0.10, -5.23)	199.58	-25.01 (-0.08, -3.46)
$(-\frac{3}{2})$	1815.27	111.60 (-0.15, 15.61)	1815.27	113.53 (-0.21, 15.65)	1815.27	116.47 (-0.13, 14.78)
	981.97	128.01 (-0.34, -41.81)	992.67	128.92 (-0.34, -40.55)	992.67	131.86 (-0.32, -38.00)
	403.57	4.75 (158.00, -9.25)	403.57	4.75 (156.69, -9.26)	403.57	5.77 (158.72, -8.75)
	213.21	-29.88 (-0.13, 2.78)	213.21	-30.79 (-0.13, 2.80)	213.21	-31.81 (-0.13, 2.64)
	202.14	-25.01 (-0.10, 6.21)	202.14	-26.03 (-0.10, 6.13)	201.79	-26.03 (-0.09, 5.29)
$(4d_{\frac{3}{2}}(m_J))$	OAM=+2					
$(+\frac{1}{2})$	2312.86	103.00 (-0.05, -1.66)	2201.13	104.92 (-0.05, -1.91)	2052.40	107.75 (-0.06, -2.15)
	1047.43	117.37 (-0.15, -5.16)	1035.53	119.30 (-0.16, -1.46)	1035.53	122.24 (-0.16, -1.43)
	405.73	13.47 (115.64, 1.51)	403.57	14.37 (86.72, 1.59)	405.73	14.37 (119.91, 1.56)
	213.21	-27.96 (-0.06, -0.55)	213.21	-28.86 (-0.07, -0.48)	213.21	-28.86 (-0.06, -0.47)
	199.66	-22.18 (-0.05, -0.71)	200.01	-23.09 (-0.05, -0.74)	199.58	-23.09 (-0.05, -0.61)
$(-\frac{1}{2})$	2559.74	101.98 (-0.04, 1.43)	2360.80	104.92 (-0.05, 1.71)	2201.13	107.75 (-0.06, 1.88)
	1035.53	117.37 (-0.16, 1.38)	1035.53	119.30 (-0.16, 1.46)	1035.53	122.24 (-0.16, 1.43)
	403.57	10.53 (82.11, -1.51)	403.57	10.53 (86.72, -1.59)	405.73	11.54 (119.91, -1.56)
	213.21	-27.96 (-0.06, 0.55)	213.21	-28.86 (-0.07, 0.48)	213.21	-28.86 (-0.06, 0.47)
	199.58	-22.18 (-0.05, 0.39)	200.01	-23.10 (-0.05, 0.74)	200.01	-23.09 (-0.05, 0.69)
$(+\frac{3}{2})$	1276.28	111.60 (-0.11, -33.13)	1276.28	112.62 (-0.11, -35.00)	1290.75	115.45 (-0.11, -28.42)
	943.34	122.24 (-0.18, 22.70)	943.34	124.17 (-0.20, 23.98)	943.34	126.99 (-0.19, 23.54)
	405.73	19.24 (115.64, 4.52)	405.73	19.24 (122.13, 4.79)	405.73	19.24 (119.91, 4.70)
	213.21	-27.96 (-0.06, -1.37)	213.21	-28.86 (-0.07, -1.45)	213.21	-28.86 (-0.06, -1.42)
	200.90	-22.18 (-0.05, -2.36)	200.90	-23.09 (-0.05, -2.50)	200.45	-23.09 (-0.05, -2.25)
$(-\frac{3}{2})$	1428.32	108.77 (-0.09, 16.18)	1451.06	109.68 (-0.09, 16.10)	1474.54	112.62 (-0.09, 14.67)
	951.22	121.22 (-0.18, -22.19)	951.22	123.15 (-0.19, -23.54)	951.22	126.99 (-0.19, -23.01)
	403.57	9.62 (82.11, -4.51)	403.57	9.62 (86.72, -4.75)	405.73	9.62 (119.91, -4.70)
	213.21	-27.96 (-0.06, 1.37)	213.21	-28.86 (-0.07, 1.45)	213.21	-28.86 (-0.06, 1.42)
	202.14	-23.09 (-0.05, 2.90)	202.14	-24.11 (-0.05, 3.06)	201.79	-24.11 (-0.05, 2.84)

TABLE II. Magic wavelengths (in nm) with corresponding polarizabilities (in a.u.) of Sr^+ for different focusing angles of the focused LG beam with OAM=+1 for the transitions $5s_{\frac{1}{2}}(+1/2) \rightarrow 4d_{\frac{5}{2}}(m_J)$. The values in the first parentheses refer vector polarizabilities of the states, $5s_{\frac{1}{2}}(+1/2)$ (left) and $4d_{\frac{5}{2}}(m_J)$ (right) at the corresponding magic wavelengths.

State ($4d_{\frac{5}{2}}(m_J)$)	Non-paraxial LG beam					
	λ^{50°	α^{50°	λ^{60°	α^{60°	λ^{70°	α^{70°
	OAM=+1					
$(+\frac{1}{2})$	1544.52	114.54 (-0.17, -4.39)	1523.86	116.47 (-0.18, -4.56)	1523.86	118.39 (-0.17, -4.31)
	1122.25	122.24 (-0.28, -5.30)	1122.25	124.17 (-0.28, -5.33)	1122.25	126.99 (-0.26, -5.46)
	403.57	18.22 (158.00, 2.14)	403.57	18.22 (156.69, 2.15)	403.57	18.22 (158.72, 2.03)
	212.22	-29.88 (-0.13, 1.44)	212.22	-29.88 (-0.13, 1.45)	212.22	-30.79 (-0.12, 1.36)
	202.14	-25.01 (-0.10, -0.89)	202.59	-26.03 (-0.10, -1.03)	202.14	-26.03 (-0.10, -0.91)
$(-\frac{1}{2})$	1656.85	113.53 (-0.16, 3.77)	1656.85	114.54 (-0.16, 3.78)	1627.26	117.37 (-0.15, 3.72)
	1122.25	122.24 (-0.28, 5.30)	1122.25	124.17 (-0.28, 5.33)	1122.25	126.99 (-0.26, 5.46)
	403.57	13.47 (158.00, -2.14)	403.57	13.47 (156.69, -2.15)	403.57	14.37 (158.72, -2.03)
	212.22	-29.88 (-0.13, -1.44)	212.22	-30.79 (-0.13, -1.45)	212.22	-30.79 (-0.12, -1.36)
	202.59	-25.01 (-0.10, 1.02)	202.59	-26.03 (-0.10, 1.03)	202.59	-26.94 (-0.10, 0.96)
$(+\frac{3}{2})$	1406.28	115.45 (-0.20, -18.64)	1428.32	117.37 (-0.20, -17.34)	1428.32	120.32 (-0.19, -16.37)
	1122.25	122.24 (-0.28 -15.94)	1122.25	124.17 (-0.28, -15.99)	1122.25	126.99 (-0.26, -15.09)
	403.57	23.09 (158.00, 6.52)	403.57	22.07 (156.69, 6.44)	403.57	22.07 (158.72, 6.10)
	212.22	-28.86 (-0.13, 4.33)	212.22	-30.79 (-0.13, 4.34)	212.22	-30.79 (-0.12, 4.10)
	201.79	-25.01 (-0.10, -2.68)	201.79	-25.01 (-0.10, -2.69)	201.79	-26.03 (-0.10, -2.56)
$(-\frac{3}{2})$	1712.91	112.62 (-0.15, 10.46)	1687.53	114.54 (-0.16, 10.86)	1687.53	117.37 (-0.15, 10.26)
	1122.25	122.24 (-0.28, 15.94)	1122.25	124.17 (-0.28, 15.99)	1122.25	126.99 (-0.26, 15.09)
	403.57	9.62 (158.00, -6.52)	403.57	9.62 (156.69, -6.44)	403.57	9.62 (158.72, -6.10)
	212.22	-29.88 (-0.13, -4.33)	212.22	-30.79 (-0.13, -4.34)	212.22	-30.79 (-0.12, -4.10)
	203.05	-26.03 (-0.10, 3.59)	203.50	-26.94 (-0.10, 4.04)	203.50	-26.94 (-0.10, 3.82)
$(+\frac{5}{2})$	1276.28	119.30 (-0.22, -46.32)	1276.28	120.32 (-0.22, -46.44)	1309.29	123.15 (-0.21, -36.17)
	1122.25	122.24 (-0.28, -26.57)	1122.25	124.17 (-0.28, -26.64)	1122.25	126.99 (-0.26, -25.16)
	403.57	26.93 (158.00, 10.70)	403.57	26.94 (156.69, 10.73)	403.57	26.94 (158.72, 10.15)
	212.22	-28.86 (-0.13, 7.23)	212.22	-30.79 (-0.13, 7.24)	212.22	-30.79 (-0.12, 6.84)
	201.79	-25.01 (-0.10, -4.48)	201.79	-26.03 (-0.10, -4.49)	201.79	-26.03 (-0.10, -4.24)
$(-\frac{5}{2})$	1687.53	112.62 (-0.16, 18.04)	1712.91	114.54 (-0.15, 17.48)	1712.91	117.37 (-0.14, 16.51)
	1122.25	122.24 (-0.28, 26.57)	1122.25	124.17 (-0.28, 26.64)	1122.25	126.99 (-0.26, 25.16)
	403.57	5.77 (158.00, -10.70)	403.57	5.77 (156.69, -10.73)	403.57	6.68 (158.72, -10.15)
	212.22	-29.88 (-0.13, -7.23)	212.22	-29.88 (-0.13, -7.24)	212.22	-30.79 (-0.12, -6.84)
	204.41	-26.03 (-0.10, 8.15)	203.95	-26.03 (-0.10, 7.46)	203.95	-26.93 (-0.10, 7.03)

-
- [1] B. Arora, M. S. Safronova, and C. W. Clark, *Phys. Rev. A* **76**, 052509 (2007).
- [2] C. Lacroûte, K. S. Choi, A. Goban, D. J. Alton, D. Ding, N. P. Stern, H. J. Kimble, *New J. Phys.* **14**, 023056 (2012).
- [3] B. Arora and B. K. Sahoo, *Phys. Rev. A* **86**, 033416 (2012).
- [4] V. V. Flambaum, V. A. Dzuba, and A. Derevianko, *Phys. Rev. Lett.* **101**, 220801 (2008).
- [5] J. Mitroy, M. S. Safronova, and C. W. Clark, *J. Phys. B: At. Mol. Opt. Phys.* **43**, 202001 (2010).
- [6] N. N. Dutta, S. Roy, and P. C. Deshmukh, *Phys. Rev. A* **92**, 052510 (2015).
- [7] A. Bhowmik, N. N. Dutta, and S. Majumder, *Phys. Rev. A* **97**, 022511 (2018).
- [8] I. Lindgren and J. Morrison, *Atomic Many-body Theory*, ed. G. E. Lambropoulos and H. Walther (3rd ed.; Berlin: Springer), 3 (1985).
- [9] R. F. Bishop, and H. G. Kummel, *Physics Today* March **40**, 52 (1987).
- [10] I. Lindgren, and J. Morrison, *Atomic Many-Body Theory*, (Springer, 1986).
- [11] I. Lindgren, *Phys. Rev. A* **31**, 1273 (1985).
- [12] R. J. Bartlett and M. Musial, *Reviews of Modern Physics* **79**, 291 (2007).
- [13] N. N. Dutta and S. Majumder *Indian Journal of Physics* **90**, 373 (2016).
- [14] A. Bhowmik, S. Roy, N. N. Dutta, and S. Majumder, *J. Phys. B: At. Mol. Opt. Phys.* **50**, 125005 (2017).
- [15] A. Das, A. Bhowmik, N. N. Dutta, and S. Majumder, *J. Phys. B: At. Mol. Opt. Phys.* **51**, 025001 (2018).
- [16] A. Kramida, Y. Ralchenko, J. Reader, and NIST ASD Team (2018). NIST Atomic Spectra Database (ver. 5.6.1), [Online]. Available: <https://physics.nist.gov/asd> [2019, September 7].
- [17] T. Kuga, Y. Torii, N. Shiokawa, and T. Hirano, *Phys. Rev. Lett.* **78**, 4713 (1997).
- [18] S. A. Kennedy, G. W. Biedermann, J. T. Farrar, T. G. Akin, S. P. Krzyzewski, and E. R. I. Abraham, *Optics Communications* **321**, 110 (2014).
- [19] J. Arlt, K. Dholakia, J. Soneson and E. M. Wright *Physical Review A* **63**, 063602 (2001).
- [20] E. M. Wright, J. Arlt, and K. Dholakia, *Phys. Rev. A* **63**, 013608 (2000).